The Fourth IEEE RAS/EMBS International Conference
on Biomedical Robotics and Biomechatronics
Roma, Italy. June 24-27, 2012

Mechanics-Based Model for Predicting In-Plane Needle Deflection with Multiple Bends

Roy J. Roesthuis, Momen Abayazid and Sarthak Misra

Abstract— **Bevel-tipped flexible needles naturally bend when inserted into soft tissue. Steering such needles along curved paths allows one to avoid anatomical obstacles and reach locations inside the human body which are unreachable with rigid needles. In this study, a mechanics-based model is presented which predicts needle deflection for a needle undergoing multiple bends during insertion into soft tissue. The model is based on a Rayleigh-Ritz formulation, and inputs to the model are a force at the needle tip and a distributed load which acts along the needle shaft. Experiments are used to evaluate the distributed load, and needle deflection is then predicted using the model. The results of the model are compared with a kinematics-based model. Maximum errors in final tip deflection are found to be 0.5 mm and 0.6 mm for the mechanics-based and kinematics-based model, respectively. Though both models are found to be comparable, the mechanics-based model can account for deflection when the needle radius of curvature is not constant (e.g., biological tissue).**

I. Introduction

Percutaneous needle insertion is one of the most common minimally invasive surgical procedures. It is often used to locally deliver drugs, perform biopsies or place radioactive seeds at specific locations within organs during brachytherapy. A problem with these procedures is that the intended target cannot always be reached by a straight path due to anatomical obstacles (e.g., blood vessels, nerves, bones) between the needle insertion point and the target. Using thin, flexible needles with asymmetric tips, instead of the traditional rigid needles, allows the needle to bend during insertion and steer around obstacles using curved paths. The possibilities of minimally invasive surgical procedures are expanded by using flexible needles, since it allows to reach locations which are not reachable with rigid needles.

Significant work on steering needles through soft tissue has been done [1], [2]. In these studies needle steering was done by maneuvring the needle base outside the tissue. This causes the soft tissue to deform and enables to place the needle tip at a desired location. Needle steering in the current work is based on the principle that a flexible needle with an asymmetric (bevel) tip naturally bends when inserted into soft tissue due to an asymmetric distribution of forces at the needle tip. By rotating the needle during insertion, the direction of bending is changed and this allows steering of the needle (Fig. 1). A number of research groups have investigated needle steering by using needles with an asymmetric (bevel) tip [3]–[10]. To be able to accurately steer such a needle around obstacles and towards a target, knowledge about needle deflection is required.

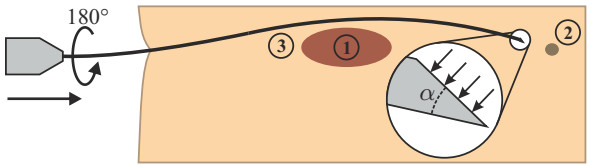

Fig. 1. A flexible needle with a bevel tip can be steered through soft tissue by performing 180° rotations during insertion. In this sketch, a flexible needle with bevel angle (α) is steered around an obstacle ①, towards a target ② by performing a rotation at ③. Models which predict the needle path are required for needle steering. Note, the force distribution at the bevel tip which causes needle deflection.

In this paper, a mechanics-based model is presented which predicts needle deflection for a needle with multiple bends. The model builds upon work presented by the authors in [11]. The salient developments in the current work are using a combination of tip force, distributed load and a series of springs to model needle-tissue interaction. This enables predicting needle deflection for multiple bends, which could not be done with the previous model. To the author's knowledge, this is the first attempt of a mechanics-based model for predicting deflection for a needle undergoing multiple bends. Such a model is required for steering around obstacles towards a target. Hence, this work contributes to research into robotically steering of flexible needles with asymmetric (bevel) tips.

Experimental deflection data is used to evaluate the distributed load along the needle shaft. The model is validated by performing a series of experiments in which the experimental needle deflection is compared with predicted needle deflection. The kinematics-based bicycle model, presented by Webster *et al*. [4], is also implemented and the results from this model are compared with the mechanics-based model.

The paper is organized as follows: Section II presents related work in the area of flexible needle insertion. Section III describes the mechanics-based model. In Section IV, the results of needle insertion experiments are presented and compared to the predicted needle deflection. The paper concludes in Section V and directions for future work are provided.

II. Related Work

Pioneering work on steering needles through soft tissue has been done by DiMaio and Salcudean [1]. They presented

The authors are affiliated with MIRA – Institute for Biomedical Technology and Technical Medicine, University of Twente, The Netherlands. This research is supported by the Dutch Technology Foundation STW, which is part of the Netherlands Organisation for Scientific Research (NWO) and partly funded by the Ministry of Economic Affairs, Agriculture and Innovation.
{r.j.roesthuis,m.abayazid,s.misra}@utwente.nl

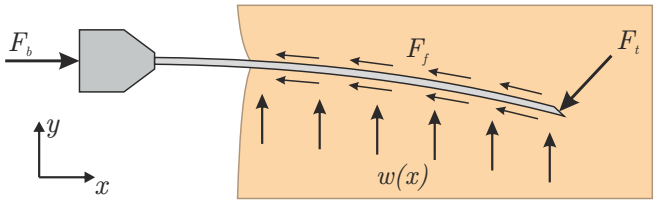

Fig. 2. When a needle with an asymmetric (bevel) tip is inserted into a soft tissue it interacts with the surrounding tissue. This is represented by forces acting on the needle: The cutting effect is modeled by an effective tip force normal to the bevel face (F_t), friction between needle shaft and tissue is represented by a friction force (F_f) along the length of the needle. Furthermore, as the needle bends it will experience resistance from the tissue, this is modeled by a distributed load $\big(w(x)\big)$. The insertion force is shown by F_b.

a needle Jacobian and maneuvred the needle base outside the tissue to position the needle tip inside the tissue. Glozman and Shoham [2] also used base maneuvring to steer the needle. They presented a virtual springs model to simulate the interaction between needle and soft tissue.

When a needle is inserted into a soft tissue, it interacts with the surrounding tissue and this causes forces which act on the needle (Fig. 2). Research on the modeling of these forces during insertion into a soft tissue has been done by a number of groups [12]–[15]. These studies consider the total insertion force at the needle base (F_b), after the tip has punctured the tissue, to be a combination of friction along the needle shaft (F_f) and cutting at the needle tip (F_t).

$$F_b = F_f + F_t. \tag{1}$$

A needle with an asymmetric tip has an uneven distribution of forces at the tip, which causes the needle to deflect from a straight path. Okamura *et al*. [15] found that needles with a bevel tip result in the largest amount of deflection compared to needles with a triangular pyramid tip or conical tip.

Both DiMaio and Salcudean, and Glozman and Shoham did not consider needle steering using the natural bending of a flexible needle with an asymmetric tip. A number of research groups investigated models which can predict needle deflection for flexible needles with a bevel tip [4], [11], [16]–[18]. Webster *et al*. [4] presented a kinematics-based approach to model needle deflection. They used the nonholonomic kinematics of a bicycle to describe the needle path (Fig. 3). Their model predicted needle deflection for a single needle rotation experimental case, with a root mean square error of 1.3 mm. The disadvantage of this kinematics-based model is that it cannot account for needle-tissue interaction. Therefore, a mechanics-based model which includes these interactions is preferred over a purely kinematics-based approach. Work on mechanics-based modeling of needle deflection has already been done by a number of research groups. Katoaka *et al*. [16] presented a model which relates forces to needle deflection. Abolhassani *et al*. [17] used tip force and a triangular load function to model needle deflection. Misra *et al*. [18] proposed an energy-based approach to approximate deflected needle shape. Tissue material properties, and needle geometrical and material properties were considered. The Rayleigh-Ritz method was used to evaluate the deflected needle shape. Roesthuis *et al*. [11] presented a

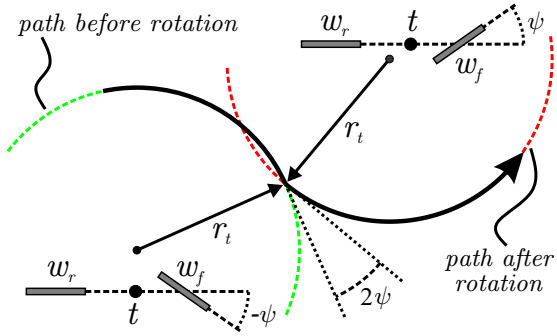

Fig. 3. Kinematics-based bicycle model: The needle tip (t) is placed in between the front wheel (w_f) and the rear wheel (w_r) of a bicycle. A fixed steering angle (ψ) results in a needle path with constant radius (r_t). Needle rotation is done by changing the sign of the steering angle: In this case from $-\psi$ to ψ. The circles describing the needle path before and after rotation are shown in green and red, respectively [4].

needle deflection model using the Rayleigh-Ritz method, in which needle tip force was used as input. A series of springs along the needle shaft were used to simulate needle-tissue interaction. However, it was found that there were limits to use the model for multiple bends. In this study the previous model is modified, instead of springs, a distributed load is proposed to model the needle-tissue interaction due to needle bending. This allows extension of the model for multiple bends. None of the prior research using a mechanics-based approach enables predicting needle deflection for a needle undergoing multiple bends. The model is validated with experiments and is compared to the kinematics-based bicycle model.

III. Mechanics-Based Model

This section presents a mechanics-based model that predicts needle deflection for a bevel-tipped needle during insertion into soft tissue. The needle is considered to bend in-plane (two-dimensional).

As previously discussed in Section II, when a needle is inserted into a soft tissue it interacts with the surrounding tissue, resulting in interaction forces. The force resulting from cutting of the tissue at the needle tip is modeled by an effective tip force (F_t) perpendicular to the bevel face (Fig. 2). As the needle bends during insertion, it will experience a resistive force from the tissue. This force is modeled by a resultant distributed load $\big(w(x)\big)$ which acts along the inserted part of the needle. In Fig. 2, this distributed load is shown as acting in the positive y-direction, but it can also act in the negative y-direction. The combination of tip force and distributed load determine the deflected needle shape. The needle is modeled as a cantilever beam, clamped at the base (x_b) in a holder outside the tissue (Fig. 4). The needle is stiff in the axial direction, therefore shortening of the needle is not considered.

The deflected needle shape $\big(v(x)\big)$ is evaluated using the Rayleigh-Ritz method. This is a variational method in which equilibrium of the system is established using the principle of minimum potential energy [19]. For any mechanical system, the system potential is expressed as

$$\Pi = U - W, \tag{2}$$

where U represents the system's potential energy, and W is the work done on the system by external forces. The Rayleigh-Ritz method requires an assumed displacement (shape) function to determine the deflected needle shape. In order to evaluate complex needle shapes (i.e. multiple bends), the needle is divided (Fig. 4(a)) into a number of elements (n), each described by their own shape function ($v_i(x)$)

$$v(x) = \begin{cases} v_i(x), & x_{i-1} \leq x \leq x_i \\ v_{i+1}(x), & x_i \leq x \leq x_{i+1} \\ \vdots & \vdots \\ v_n(x), & x_{n-1} \leq x \leq x_n \end{cases}. \tag{3}$$

Each element is described by a cubic shape function

$$v_i(x) = a_{0,i} + a_{1,i}x + a_{2,i}x^2 + a_{3,i}x^3, \tag{4}$$

where $a_{0,i} \dots a_{3,i}$ are the shape functions' coefficients of the i-th element. For the first needle element ($i = 1$), x_{i-1} equals x_b, and for the last element ($i = n$), x_i equals x_t. Each of the shape functions (3) has to satisfy the geometric boundary conditions of the system. Since the needle is fixed at the base (x_b), the following boundary conditions are applied

$$v_1(x_b) = 0 \text{ and } \theta_1(x_b) = \frac{dv_1}{dx}|_{x=x_b} = 0, \tag{5}$$

meaning zero deflection and zero needle slope (θ) at the needle base. Furthermore, the shape functions have to satisfy continuity conditions, meaning continuous deflection and needle slope at the boundaries of the elements

$$v_i(x_i) = v_{i+1}(x_i) \text{ and } \theta_i(x_i) = \theta_{i+1}(x_i). \tag{6}$$

Since only transversal needle deflection is considered, the transversal component of the tip force ($F_{t,y}$) is required (Fig. 4). The transversal tip force is related to tip force by bevel angle (α) and needle tip slope (θ_t)

$$F_{t,y} = F_t \cos(\alpha + \theta_t). \tag{7}$$

When the needle is not rotated during insertion, the needle has a *single bend* shape (Fig. 4(a)). The system potential for this case is written as

$$\Pi = \underbrace{U_b}_{U} - \underbrace{(W_c + W_d)}_{W}, \tag{8}$$

where U_b is the strain energy associated with transversal needle bending, W_c is the work done by transversal tip force and W_d is the work done by the distributed load. Using Euler-Bernoulli beam theory [20], the strain energy for transversal beam bending (U_b) is calculated using

$$U_b = \frac{EI}{2} \int_{x_b}^{x_t} \left(\frac{d^2 v(x)}{dx^2} \right)^2 \mathrm{d}x, \tag{9}$$

where E (Pa) and I (m^4) are the Young's modulus and second moment of inertia of the needle, respectively. The work done by transversal tip force ($F_{t,y}$) is given by

$$W_c = F_{t,y} v(x_t), \tag{10}$$

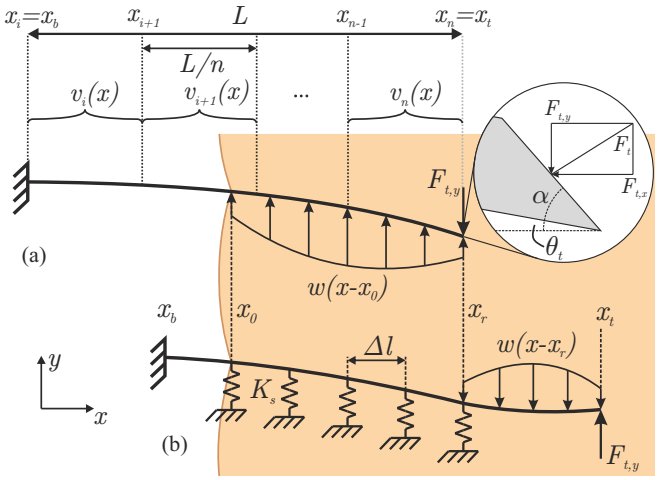

Fig. 4. Mechanics-based model: The needle is modeled as a cantilever beam and divided into n elements, each described by their own shape function $(v_i(x))$. (a) In the case of a *single bend* needle shape, the needle deflects due to a combination of needle tip force $(F_{t,y})$ and distributed load $(w(x))$. (b) Needle rotation is performed at x_r, causing the tip force to change direction. This results in the needle to deflect in the opposite direction. The *double bend* needle shape is modeled by fixing the part of the needle before rotation ($x_0 \leq x \leq x_r$) with a series of springs.

where $v(x_t)$ is the deflection at the needle tip. The work done by the distributed load ($w(x)$) is given by

$$W_d = \int_{x_0}^{x_t} (w(x)v(x))\,\mathrm{d}x. \tag{11}$$

When the needle is rotated during insertion, the orientation of the bevel tip changes and causes the needle to bend in the opposite direction. A single needle rotation results in the needle having a *double bend* shape (Fig. 4(b)). This *double bend* needle shape is modeled by fixing the part of the needle before rotation ($x_0 \leq x \leq x_r$) with a series of springs. This means that this part of the needle ($x_0 \leq x \leq x_r$) is resting on an elastic foundation. An elastic foundation can be approximated by a series of springs if the spacing (Δl) between the springs is sufficiently small [21]. The stiffness of the elastic foundation per unit length is given by K_0 ($\mathrm{N/mm}^2$). This stiffness depends on tissue elasticity, and needle and tissue geometric properties. The stiffness of the foundation (K_T) for a rotation at x_r is calculated by

$$K_T = K_0 (x_r - x_0). \tag{12}$$

For a total number of m springs, the individual spring stiffness (K_s) is calculated as

$$K_s = \frac{K_T}{m}. \tag{13}$$

Due to the elastic foundation, an additional term (U_s) needs to be included in the system potential (8)

$$\Pi = \underbrace{(U_b + U_s)}_{U} - \underbrace{(W_c + W_d)}_{W}, \tag{14}$$

where U_s represents the potential energy stored in the springs

$$U_s = \sum_{k=1}^{m} \frac{1}{2} K_s v(x_k)^2, \tag{15}$$

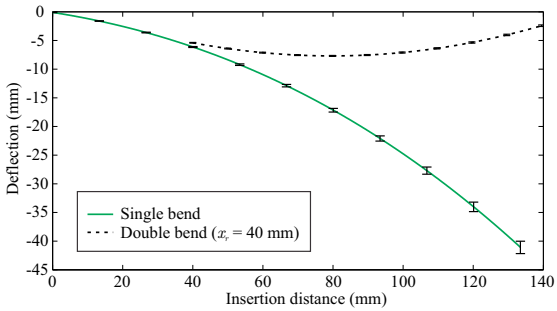

Fig. 5. Deflection for *single bend* and *double bend* experiments. Five insertions are performed for each experiment. The errorbars represent the standard deviation. Average final tip deflection is -41.1 mm (σ = 1.1 mm) and -2.4 mm (σ = 0.1 mm) for *single bend* and *double bend*, respectively.

where $v(x_k)$ is the deflection of the k-th spring with respect to the bent shape as shown in Fig. 4(b).

The assumed shape functions defined in (3) are substituted in the expressions for the energy and work terms in (9), (10), (11) and (15). This results in the system potential being a function of the coefficients defining the shape functions

$$\Pi = f(a_{0,i}, a_{1,i}, a_{2,i}, a_{3,i}). \tag{16}$$

The equilibrium of the system is found by taking the partial derivative of the system potential for each of the coefficients

$$\frac{\partial \Pi}{\partial a_{j,i}} = 0, \tag{17}$$

for $j = 0, 1, 2, 3$ and $i = 1 \ldots n$. The coefficients $a_{j,i}$ are calculated by solving the system of equations in (17). Substituting the coefficients back into (4) then gives the deflected needle shape. Extension of the model to multiple bends is possible by fixing the needle with a series of springs after each rotation and applying the appropriate distributed load.

IV. Experimental Results

This section presents the results of needle insertion experiments. First, experiments are performed to evaluate the distributed load ($w(x)$) for the needle having a *single bend* and *double bend* shape. With the distributed loads known, the mechanics-based model is then used to predict needle deflection in experiments for different multiple bend cases. Needle deflection is also predicted using the kinematics-based bicycle model, and these results are compared with the mechanics-based model.

A. Materials and Methods

In the experiments, gelatine is used a soft-tissue simulant. Gelatine phantoms are made by mixing 14.9% gelatine powder with 85.1% water. Tissue elasticity was determined using an Anton Paar Physica MCR501 (Anton Paar GmbH, Graz, Austria) and is found to be 35 kPa. This value is within the range that is found in a human breast [22]. Needle insertions are performed using a Nitinol needle (E = 75 GPa) with a 30° bevel angle (α) and a diameter of ϕ 0.8 mm. A two degree of freedom (DOF) needle insertion device is used to insert the needles into the gelatine phantoms [11]. The experimental setup allows translation of the needle along and rotation about the needle's longitudinal axis. The needle is inserted at a velocity of 10 mm/s. Experiments have shown that varying insertion velocity between 5 mm/s and 25 mm/s only results in a small change in needle deflection [23]. Each insertion is done at a new location in the phantom to avoid influence of a previous insertion. Videos of the experiments are recorded using a Sony XCD-SX90 FireWire camera (Sony Corporation, Tokyo, Japan) mounted 450 mm above the phantom. After the insertion, a corner detection algorithm is used to detect the needle tip [11].

B. Model Fitting

The mechanics-based model requires transversal tip force ($F_{t,y}$) and distributed load $\big(w(x)\big)$ as inputs. Measuring tip force directly during insertion is not possible since the insertion force (1) is a combination of tip force and friction force. In [11], we have already shown a method of estimating the tip force by determining the needle friction force. We found that the tip force for a ϕ 1.0 mm diameter needle was 0.40 N. Moreover, it was observed that tip force was almost constant during insertion. Therefore, the effect of changing needle slope on the tip force (7) is neglected here and a constant tip force is used. Misra *et al*. [18] showed that the magnitude of the tip force scales proportionally with the bevel surface area. Therefore, it is assumed that the tip force for a ϕ 0.8 mm needle is 0.25 N ($\frac{0.8^2}{1.0^2} \times 0.40$).

The distributed load is evaluated by fitting the model to experimental deflection data. This fitting is done by minimizing the error (ε) between simulated needle deflection $\big(v_{sim}(x)\big)$ and experimental needle deflection $\big(v_{exp}(x)\big)$

$$\varepsilon = \varepsilon_1 + \varepsilon_2, \tag{18}$$

where ε_1 is the difference in deflection along the needle shaft

$$\varepsilon_1 = \frac{1}{x_t - x_0} \int_{x_0}^{x_t} \left(v_{exp}(x) - v_{sim}(x)\right)^2 \mathrm{d}x, \tag{19}$$

and ε_2 is the difference in deflection at the needle tip

$$\varepsilon_2 = \left(v_{exp}(x_t) - v_{sim}(x_t)\right)^2. \tag{20}$$

Since the profile of the distributed load ($w(x)$) is unknown, several load profiles are evaluated (e.g., constant, linear and quadratic loads). It is found that a cubic load profile gives the best fit with the experimental deflection

$$w(x) = b_0 + b_1 x + b_2 x^2 + b_3 x^3. \tag{21}$$

The error (18) is minimized to evaluate the coefficients ($b_0, \ldots, b_3$). Both *single bend* and *double bend* experiments (Fig. 5) are performed to evaluate the distributed load. In both experiments, the Nitinol needle is inserted a total distance of 140 mm. For the *double bend* experiment, needle rotation is performed at an insertion distance of 40 mm. Variation in deflection between insertions is most likely caused by differences in initial needle orientation.

In order to simulate the *double bend* needle shape, the stiffness of the elastic foundation per unit length (K_0) needs to be known. For the needle-tissue combination used here, $K_0 = 0.15$ N/mm^2 gives the best fit to experimental

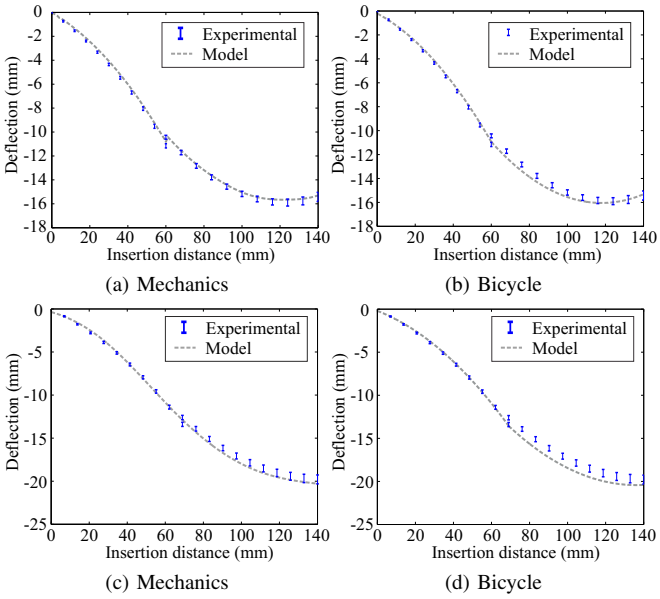

Fig. 6. Comparing predicted needle deflection between the mechanics-based model ((a),(c)) and the kinematics-based bicycle model ((b),(d)) for experimental needle rotation at 60 mm ((a),(b)) and 69 mm ((c),(d)). Five insertions are done for each experiment.

deflection. The total number of elements (n) in the model in chosen to be 3 and 5 for the *single bend* and *double bend* experiments, respectively. Choosing a larger number of elements did not influence the needle shape.

The predicted needle deflection using the mechanics-based model is compared with the kinematics-based bicycle model. To evaluate the bicycle model, the steering angle (ψ) and the radius of the circle describing the needle path (r_t) need to be determined. The radius of curvature is determined by fitting a circle to the experimental deflection using a method described by Pratt *et al.* [24] and is found to be 332.4 mm (σ = 13.4 mm) for the *single bend* experiment (Fig. 5). The steering angle is determined by fitting the model to the deflection of the *double bend* experiment (Fig. 5) and is found to be 2.7°.

With the parameters known for the mechanics-based model and the kinematics-based bicycle model, it is now possible to predict needle deflection. In the next section, both models are evaluated for multiple bend experiments.

C. Model Validation

First, two *double bend* experiments are performed. The needle is inserted a total distance of 140 mm at 10 mm/s. Needle rotation is performed at insertion distances of 60 mm and 69 mm, in the first and second experiment, respectively.

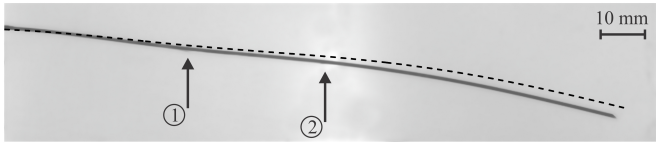

Fig. 7. Image showing the deflected needle (ϕ = 0.8 mm) for rotations performed at ① 40 mm and ② 71 mm. The dashed line represents the predicted needle deflection using the mechanics-based model. Average needle tip deflection is 21.0 mm (σ = 0.3 mm) and predicted needle tip deflection is 18.3 mm, indicating a tip error of 2.7 mm.

For each experiment five insertions are done. Both the mechanics-based and the kinematics-based bicycle model are evaluated for these rotation distances using the parameters determined in the previous section. The predicted needle deflection is compared with the experimental needle deflection in Fig. 6. The differences between predicted and experimental final needle tip deflection are presented in Table I. It can be seen that both models are accurate in predicting needle deflection. The maximum errors in final tip deflection are 0.5 mm and 0.6 mm for the mechanics-based and kinematics-based model, respectively. The maximum error is larger for the kinematics-based model: 1.1 mm as compared to 0.6 mm for the mechanics-based model.

The mechanics-based model is also evaluated when the needle is rotated twice during insertion (*triple bend*). The same Nitinol needle (ϕ = 0.8 mm) is used and rotation is performed at insertion distances of 40 mm and 71 mm (Fig. 7). The needle appears to be almost straight in the image. This is due to the limited amount of curvature for this needle, resulting in an almost straight shape when two or more rotations are performed. The predicted needle shape is similar to the experimental shape. Gelatine is observed to become stiff with time, which affects the amount of needle deflection. The tip error for the *triple bend* experiments is larger than for the experiments in Fig. 6. This is probably caused by the fact the model (used for the *triple bend* experiments) are fitted to experiments done on different days.

V. Conclusions and Future Work

This study presents a mechanics-based model for a needle undergoing multiple bends. The model is based on a Rayleigh-Ritz formulation where shape functions are assumed for the deflected needle. The unknown coefficients of the shape functions are evaluated by minimizing the sytem potential. The system potential consists of energy terms due to needle bending and needle-tissue interaction, and work terms due to forces acting on the needle. The forces are at the needle tip due to cutting of the tissue, and a distributed load along the needle shaft which accounts for the force applied by the surrounding tissue as the needle bends.

TABLE I

Experiments compared with predicted needle deflection using the mechanics-based model and the kinematics-based bicycle model. Note, rotation distance (x_r), experimental tip deflection ($y_{T,exp}$), predicted needle tip deflection ($y_{T,sim}$), tip error ($e(x_T)$), maximum error (e_{max}) and the standard deviation of final tip deflection ($\sigma(x_T)$).

Model	x_r (mm)	$y_{T,exp}$ (mm)	$y_{T,sim}$ (mm)	$e(x_T)$ (mm)	e_{max} (mm)	$\sigma(x_T)$ (mm)
Mechanics	60	-15.4	-15.3	0.1	0.3	0.4
	69	-19.8	-20.3	0.5	0.6	0.5
Bicycle	60	-15.4	-15.3	0.1	0.5	0.4
	69	-19.8	-20.4	0.6	1.1	0.5

A. Conclusions

The mechanics-based model presented in this work requires the tip force and the distributed load as inputs. Experiments are performed using a flexible, Nitinol needle (ϕ 0.8 mm) with a bevel tip. Gelatine is used as soft tissue simulant. The tip force is considered constant during insertion, while the distributed load is evaluated by fitting the model to experimental data. *Double bend* experiments are performed to validate the model. We are able to predict deflection for a needle undergoing a *double bend* with a maximum tip error of 0.5 mm. The kinematics-based bicycle model is also implemented and results in a maximum tip error of 0.6 mm. The maximum error observed is smaller for the mechanics-based model: 0.6 mm as compared to 1.1 mm for the kinematics-based model. The mechanics-based model is also evaluated for a *triple bend* experiment, and shows good agreement with experimental needle deflection. These results indicate that the mechanics-based model and kinematics-based bicycle model are comparable for predicting delfection for needles with multiple bends in homogeneous soft-tissue simulants. Though, the mechanics-based model can account for deflection when the needle radius of curvature is not constant. This is especially advantageous for predicting needle deflection in non-homogeneous biological tissue.

B. Future Work

In the current study, the distributed load is evaluated for a single needle-tissue combination. For the triple bend case, it was shown that needle deflection is sensitive to changes in gel stiffness and the prediction is not quite accurate anymore. Therefore, research into the distrituted load for different needles and soft-tissue simulants is required. Knowledge about the relationship between distributed load, and needle and tissue properties would enable predicting needle deflection without having to fit the model to experimental data.

The model assumes in-plane (two dimensional) needle deflection. Predicting needle deflection for the three dimensional case using the presented framework is possible. For this, the distributed load has to be adapted such that it acts in all three directions.

The mechanics-based model presented has shown to predict deflection for a needle undergoing multiple bends. Such a model is required to accurately steer needles in robot-assisted needle insertion procedures where knowledge about needle deflection is required for both path-planning before the procedure, and control during the procedure.

REFERENCES

[1] S. DiMaio and S. Salcudean, "Needle steering and model-based trajectory planning," in *Proceedings of the International Conference Medical Image Computing and Computer-Assisted Intervention (MICCAI)*, vol. 2878, (Montreal, Canada), pp. 33–40, September 2003.

[2] D. Glozman and M. Shoham, "Image-guided robotic flexible needle steering," *IEEE Transactions on Robotics*, vol. 23, no. 3, pp. 459–467, 2007.

[3] R. Alterovitz, K. Goldberg, and A. M. Okamura, "Planning for steerable bevel-tip needle insertion through 2d soft tissue with obstacles," in *Proceedings International Conference of Robotics and Automation (ICRA)*, (Barcelona, Spain), pp. 1640–1645, Apr. 2005.

[4] R. J. Webster III, J. S. Kim, N. J. Cowan, G. S. Chirikjian, and A. M. Okamura, "Nonholonomic modeling of needle steering," *International Journal of Robotics Research*, vol. 25, no. 5-6, pp. 509–525, 2006.

[5] J. A. Engh, G. Podnar, D. Kondziolka, and C. N. Riviere, "Toward effective needle steering in brain tissue," in *Proceedings of the 28th IEEE International Conference in Medicine and Biology Society (EMBS)*, (New York City, USA), pp. 559–562, Aug. - Sept. 2006.

[6] N. Abolhassani, R. V. Patel, and M. Moallem, "Needle insertion into soft tissue: A survey," *Medical Engineering and Physics*, vol. 29, no. 4, pp. 413–431, 2007.

[7] V. Duindam, R. Alterovitz, S. Sastry, and K. Goldberg, "Screw-based motion planning for bevel-tip flexible needles in 3d environments with obstacles," in *Proceedings IEEE International Conference of Robotics and Automation (ICRA)*, (Pasadena, USA), pp. 2483–2488, May 2008.

[8] V. Kallem and N. J. Cowan, "Image guidance of flexible tip-steerable needles," *IEEE Transactions on Robotics*, vol. 25, no. 1, pp. 191–196, 2009.

[9] N. A. Wood, K. Shahrour, M. C. Ost, and C. N. Riviere, "Needle steering system using duty-cycled rotation for percutaneous kidney access," in *Proceedings IEEE International Conference of Medicine and Biology Society (EMBC)*, (Buenos Aires, Argentina), pp. 5432–5435, Aug. - Sep. 2010.

[10] K. Reed, A. Majewicz, V. Kallem, R. Alterovitz, K. Goldberg, N. Cowan, and A. Okamura, "Robot-assisted needle steering," *IEEE Robotics and Automation Magazine*, vol. 18, no. 4, pp. 35 –46, 2011.

[11] R. J. Roesthuis, Y. R. Van Veen, A. Jahya, and S. Misra, "Mechanics of needle-tissue interaction," in *Proceedings IEEE International Conference of Intelligent Robots and Systems (IROS)*, (San Francisco, USA), pp. 2557 – 2563, Sep. 2011.

[12] H. Kataoka, T. Washio, K. Chinzei, K. Mizuhara, C. Simone, and A. M. Okamura, "Measurement of the tip and friction force acting on a needle during penetration," in *Proceedings of the International Conference Medical Image Computing and Computer-Assisted Intervention (MICCAI)*, (London, UK), pp. 216–223, Sep. 2002.

[13] C. Simone and A. M. Okamura, "Modeling of needle insertion forces for robot-assisted percutaneous therapy," in *Proceedings of the IEEE International Conference of Robotics and Automation (ICRA)*, (Washington, USA), pp. 2085–2091, May 2002.

[14] M. D. O'Leary, C. Simone, T. Washio, K. Yoshinaka, and A. M. Okamura, "Robotic needle insertion: Effects of friction and needle geometry," in *Proceedings of the IEEE International Conference of Robotics and Automation (ICRA)*, (Taipei, Taiwan), pp. 1774–1780, Sep. 2003.

[15] A. M. Okamura, C. Simone, and M. D. O'Leary, "Force modeling for needle insertion into soft tissue," *IEEE Transactions on Biomedical Engineering*, vol. 51, no. 10, pp. 1707–1716, 2004.

[16] H. Kataoka, T. Washio, M. Audette, and K. Mizuhara, "A model for relations between needle deflection, force, and thickness on needle penetration," in *Proceedings of the 4th International Conference Medical Image Computing and Computer-Assisted Intervention (MICCAI)*, vol. 2208, (Utrecht, The Netherlands), pp. 966–974, Oct. 2001.

[17] N. Abolhassani and R. V. Patel, "Deflection of a flexible needle during insertion into soft tissue," in *Proceedings of the 28th IEEE International Conference in Medicine and Biology Society (EMBS)*, (New York City, USA), pp. 3858–3861, Aug.- Sep. 2006.

[18] S. Misra, K. B. Reed, B. W. Schafer, K. T. Ramesh, and A. M. Okamura, "Mechanics of flexible needles robotically steered through soft tissue," *International Journal of Robotics Research*, vol. 29, no. 13, pp. 1640–1660, 2010.

[19] O. Bauchau and J. Craig, *Structural Analysis*. Springer, 2009.

[20] R. C. Hibbeler, *Mechanics of Materials*. Prentice Hall, 2008.

[21] E. S. Melerski, *Design Analysis Beams Circular Plates and Cylindrical Tanks on Elastic Foundations*. Taylor & Francis, 2000.

[22] A. Gefen and B. Dilmoney, "Mechanics of the normal woman's breast," *Technology and Health Care*, vol. 15, no. 4, pp. 259–271, 2007.

[23] Y. R. J. van Veen, A. Jahya, and S. Misra, "Macroscopic and microscopic observations of needle insertion into gels," *Proceedings of the Institute of Mechanical Engineering Part H, Journal of Engineering in Medicine*, 2012. In Press.

[24] V. Pratt, "Direct least-squares fitting of algebraic surfaces.," *Computer Graphics (ACM)*, vol. 21, no. 4, pp. 145–152, 1987.